

**NASA TECHNICAL
MEMORANDUM**

NASA TM X-71584

NASA TM X-71584

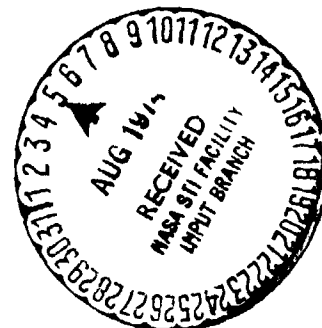
(NASA-TM-X-71584) TRACTION AND FILM
THICKNESS MEASUREMENTS UNDER STARVED
ELASTOHYDRODYNAMIC CONDITIONS (NASA) 35 p
HC \$3.25 CSCI 11H

N74-29929

Unclas
G3/15 54441

**TRACTION AND FILM THICKNESS MEASUREMENTS
UNDER STARVED ELASTOHYDRODYNAMIC CONDITIONS**

by L. D. Wedeven
Lewis Research Center
Cleveland, Ohio 44135



TECHNICAL PAPER proposed for presentation at
Lubrication Conference sponsored by the American Society
of Mechanical Engineers and American Society of
Lubrication Engineers
Montreal, Canada, October 8-10, 1974

TRACTION AND FILM THICKNESS MEASUREMENTS UNDER
STARVED ELASTOHYDRODYNAMIC CONDITIONS

L. D. Wedeven

National Aeronautics and Space Administration
Lewis Research Center
Cleveland, Ohio 44135

ABSTRACT

Traction measurements under starved elastohydrodynamic conditions have been obtained for a point contact geometry. Simultaneous measurements of the film thickness and the location of the inlet lubricant boundary were made optically. The thickness of a starved film for combination rolling and sliding conditions varies with the location of the inlet boundary in the same way found previously for pure rolling.

A starved film was observed to possess greater traction than a flooded film for the same slide roll ratio. For a given slide roll ratio a starved film simply increases the shear rate in the Hertz region. The maximum shear rate depends on the degree of starvation and has no theoretical limit. The relative increase in traction due to starvation is influenced by thermal and fluid rheological conditions within the Hertz region. This makes the prediction of traction under starved conditions difficult. Traction measurements under starved conditions were compared with flooded conditions under equivalent shear rates in the Hertz region. When the shear rates in the Hertz region were low and the film severely starved, the measured tractions were found to be much lower than expected.

E-8036

LIST OF SYMBOLS

- a = Hertzian radius
 E_1, E_2 = modulus of elasticity of ball and transparent disk materials
 E' = reduced elastic modulus;

$$\frac{1}{E'} = \frac{1}{2} \left(\frac{1-\sigma_1^2}{E_1} + \frac{1-\sigma_2^2}{E_2} \right)$$

- h = film thickness
 h_b = film thickness at the inlet lubricant boundary
 h_o = film thickness at the center of the Hertz region
 $(h_o)_f$ = central film thickness under flooded conditions
 h_r = film thickness at the rear constriction
 h_s = film thickness at the side constrictions
 R_1, R_2 = radius of contacting bodies of ball and disk
R = reduced radius of contact;

$$\frac{1}{R} = \frac{1}{R_1} + \frac{1}{R_2}$$

- S = inlet distance measured from inlet lubricant boundary to leading edge of Hertz region
 S_f = inlet distance necessary to obtain a flooded film thickness
 u_1 = surface velocity of ball
 u_2 = surface velocity of disk
 \bar{u} = rolling velocity;

$$\bar{u} = \frac{1}{2} (u_1 + u_2)$$

- x = coordinate
- α = pressure viscosity coefficient
- σ_1, σ_2 = Poisson's ratio of ball and disk materials
- μ = local viscosity of lubricant
- μ_0 = ambient viscosity of lubricant

DIMENSIONLESS GROUPS

- $\frac{h}{h_0}$ = dimensionless gap thickness
- $\frac{h_b}{h_0}$ = dimensionless gap thickness at inlet lubricant boundary
- $\frac{h_0}{(h_0)_f}$ = ratio of starved to flooded film thickness
- $\frac{h - h_0}{h^3}$ = geometry term
- $\frac{S}{S_f}$ = starvation parameter;
- $$\frac{S}{S_f} = \frac{S a^{1/3}}{3.52 [R(h_0)_f]^{2/3}}$$
- $\frac{u_1 - u_2}{\frac{1}{2}(u_1 + u_2)}$ = slide roll ratio
- $\frac{u_1 - u_2}{h_0}$ = apparent shear rate

INTRODUCTION

The elastohydrodynamic (EHD) lubrication of gears and bearings results from the generation of pressure between surfaces in relative motion. The pressure generation, which can be described by Reynolds equation, occurs predominately in the region where the surfaces are in close proximity. The most important parameter from a lubrication point of view is the surface separation, or film thickness, which is developed under the given conditions of operation. In general, the operating conditions of concern are: the load, the relative surface velocity, the surface geometry, and the controlling lubricant viscosity. Another operating condition which may frequently be important but rarely considered is the supply and distribution of lubricant in the neighborhood of the conjunction region. The supply of lubricant determines the upstream boundary or limit where hydrodynamic pressure is allowed to commence. When the upstream fluid boundary protrudes into the vicinity of the conjunction region, it inhibits the generation of hydrodynamic pressure. This alters the elastohydrodynamic behavior of the system in several important ways. For example, it has been shown that starvation lowers the film thickness [1,2,3].¹ It also lowers the rolling friction [4]. In addition, when the surfaces are in relative sliding, starvation is expected to increase the sliding friction, or traction force, transmitted by the lubricant film. In practice the effects of starvation may be beneficial as well as detrimental. In either case, the influence of starvation can be an overriding factor on the performance of machine elements [5,6,7,8]. It is the purpose of this paper to consider the effect of starvation on film thickness and traction under conditions of rolling and sliding.

¹Numbers in brackets designate references at end of paper

BACKGROUND

The influence of starvation can best be understood by considering certain predominant features and regions of the EHD problem. Perhaps the most characteristic feature of the EHD problem is its near Hertzian pressure distribution and elastic deformation. This allows the EHD conjunction to be divided up into three general regions as shown in Fig. 1.

Inlet Region

If the side leakage term in Reynolds equation is neglected, it can be integrated with respect to x to give

$$\frac{dp}{dx} = 12 \bar{u} \mu \left(\frac{h-h_0}{h^3} \right)$$

where p is the pressure generated in the film of thickness h , μ is the local viscosity, \bar{u} is the rolling velocity and h_0 is the film thickness at maximum pressure.

The importance of the inlet region to lubrication can be seen by considering the geometry term $(h-h_0)/h^3$ in the integrated form of Reynolds equation. For a constant velocity \bar{u} and lubricant viscosity μ the rate of pressure generation dp/dx is a function of this geometry term. If we look at the value of the geometry term, we will see that the hydrodynamic pressure generation is essentially confined to the inlet region. Fig. 2 shows the value of the geometry term at various positions within the inlet region. The location within the inlet region is expressed in terms of h/h_0 which is the thickness of the inlet gap relative to the film thickness in the center of the Hertz region. Significant values of the geometry term occur within a gap ratio between 1 and 9 reaching a maximum at 1.5. Since the pressure generation is directly related to the

geometry term it then follows that the hydrodynamic pressure is mostly generated within the inlet region where the inlet gap thickness is between 1 and 9 times the central film thickness. It is the pressure generated in this region that establishes the film thickness h_0 which is observed in the Hertz region. The gap ratio h/h_0 is a very important parameter in connection with starvation.

Hertz Region

The Hertz region is dominated by the Hertzian pressure. This is the pressure that would exist if the surfaces were not separated by a lubricant film. The actual pressure differs from this Hertzian pressure only at the leading and trailing edges of the Hertz region. Because the lubricant encounters very high pressures in the Hertz region, its viscosity will increase several orders of magnitude. This, along with the very thin parallel film in the Hertzian region, is the major cause of friction or traction between the bearing surfaces when they are in relative sliding.

Exit Region

The exit region exposes the fluid to a rapidly diverging geometry which produces a negative pressure gradient and eventually subambient pressures. Since most fluids degas or cavitate under relatively low tensile stresses, this subambient hydrodynamic pressure is almost immediately terminated.

In brief, each of the three regions as described above performs a particular function. The inlet region "pumps the film up", the Hertz region "rides it" and the exit region "discharges it". It is convenient to consider the influence of starvation on film thickness and traction in terms of these regions.

EXPERIMENTAL APPARATUS

Ball and Disk Materials

Measurements of film thickness and traction were obtained from a nominal point contact geometry. The bearing components which are shown in Fig. 3 consist of a 0.02063 meter (0.8125 in) diameter ball which rides against a flat transparent disk. To obtain a range of maximum Hertzian pressures both steel and tungsten carbide were used for ball materials and quartz and sapphire were used as disk materials. Their mechanical properties are shown in Table I and the reduced elastic modulus (E') of each material combination is shown in Fig. 4.

Lubricant Supply

The ball is supported by three bearings as shown in Fig. 3. The three bearings are contained within a lubricant reservoir. The spaces around the bearings are filled with the test lubricant. When the reservoir is completely filled, the ball is partially submerged in the test lubricant. The required lubricant supply for the starvation tests was achieved by limiting the lubricant supply in the reservoir. The motion of the support bearings within the reservoir very conveniently carries the test lubricant to the test ball surface adjacent to the track on the ball. This method provided a uniform and steady inlet meniscus. An air cylinder below the lubricant reservoir provided the required test load on the ball.

Drive Mechanism and Speed Control

The assembled apparatus is shown in Fig. 5. The ball is driven by a 1/5 hp electric motor through the gearbox which has the ratios 1:1, 10:1, and 100:1. The motor is a variable speed motor-generator with a very

stable transistorized closed-loop control system. Speed regulation is much better than 1 percent.

Measurement of ball speed was achieved with a magnetic transducer in close proximity to a 100 tooth gear wheel attached to the motor shaft. The motor speed was displayed on a digital counter.

Torque Control and Disk Speed Measurement

A controlled braking torque was applied to the rotating transparent disk with a dynamometer which uses a hysteresis brake. The unique feature of the hysteresis brake is that it provides a constant torque independent of shaft speed. To obtain accurate slip measurements between the ball and disk it is important that the disk speed be measured accurately. This was achieved by using an optical transducer in conjunction with a 600 element encoder disk. The disk speed was displayed on a digital counter and also recorded on a 4-pen recorder.

Traction Measurement

The traction force between the bearing surfaces was obtained by measuring the reaction force on the ball. The motor, gearbox and loading cylinder were suspended on an air bearing which is pivoted on one end and restrained by beryllium springs on the other end. The reaction force on the ball is directly proportional to the deflection of the beryllium springs. The deflection of the springs was measured with a capacitance transducer and displayed on a 4-pen recorder.

Film Thickness Measurement

The EHD film thickness was measured using optical interferometry. Fringes of very good visibility were obtained by using a 17 percent reflect-

ing layer of chromium on the bearing surface of the transparent disks. Interference measurements were made using wavelengths of two colors (red and green). These were obtained by using a special filter and a Xenon flash lamp as a light source. The details of this system and its calibration are described for fully in references [1] and [9].

Film thickness measurements under starved conditions were taken from high-speed photomicrographs using a high-speed 35 mm color film. The traction and disk speed corresponding to the photomicrograph was marked by one of 4 pens on the 4-pen recorder using a synchronized pulse from the Xenon flash power supply. Typical photomicrographs with varying degrees of starvation are shown in Fig. 6.

TEST LUBRICANT

The traction/starvation tests were performed with a synthetic paraffinic oil. It is synthesized by the polymerization of a relatively pure mono-olefin so that it can be considered a single chemical species composed of molecules of a chain length distribution depending on the degree of polymerization. Some of its properties are listed in Table 2. The variation of viscosity with temperature, pressure and shear stress is reported in reference [10]. This fluid has also been examined in disk machines for film thicknesses [11] and traction [12]; and it has been tested in various full-scale bearing tests [13-16].

TEST CONDITIONS

Starvation/traction measurements were performed under three nominal test conditions each with a different set of material combinations to obtain three different maximum Hertzian pressures: $.496 \times 10^9 \text{ N/m}^2$

(72,000 psi), 1.21×10^9 N/m² (175,000 psi) and 1.9×10^9 N/m² (275,000 psi). The corresponding material combinations are respectively: quartz/steel, sapphire/steel, and sapphire/tungsten carbide. Although the maximum Hertzian pressures for each test vary a great deal, the material combinations provide similar elastic deformations. This can be seen in Table 3, where the Hertzian radius "a" along with other test parameters are given for each of the three test conditions. Thus, the departure from the true Hertzian condition for each test is approximately the same since they were all performed at essentially the same flooded film thickness.

Each test was performed with the flooded film thickness corresponding to a particular interference fringe (3rd red fringe). The actual film thickness which is given in Table 3 varies slightly for each test because the refractive index of the test fluid increases with pressure. There are eight fringes below the 3rd red fringe from which measurements could be made when the film was starved. The two color interferometric system allows easy interpolation between fringes.

TEST PROCEDURE

Prior to each test, the bearing components shown in Fig. 3 were cleaned with Freon. The parts were assembled and the lubricant reservoir was filled with the test fluid. The ball was loaded against the transparent disk and driven at a speed which would establish the 3rd red fringe in the center of the Hertzian region. The rotational velocities of the ball and disk were then recorded. To maintain a constant rolling velocity ($\bar{u} = 1/2 (u_1 + u_2)$) during a traction run a plot of the ball velocity versus disk velocity for a constant rolling velocity (\bar{u}) was then made.

A constant brake force from the hysteresis brake was then applied to the disk and the ball velocity was adjusted to maintain a constant \bar{u} . A 4-pen recorder recorded the traction force, disk velocity and temperature. The temperature was that of the test chamber which was measured with a Chromel-Constantan thermocouple. All tests were performed at room temperature.

Under fully flooded inlet conditions the ball and disk velocities were recorded for each brake torque applied to the disk. The brake torque was increased incrementally until 100 percent sliding (zero disk velocity) was achieved.

Starved inlet conditions were obtained by gradually depleting the lubricant supply in the reservoir and on the transparent disk. Under starved inlet conditions a high-speed photomicrograph was taken for each brake force applied. The film thickness and the location of the inlet meniscus were determined from the photomicrographs.

STARVATION AND FILM THICKNESS FOR ROLLING AND SLIDING

The influence of the location of the inlet lubricant boundary (starvation) on film thickness has been shown theoretically for conditions of point [1] and line [2-4] contact. In addition, these solutions have been verified experimentally [1,17] under conditions of pure rolling.

When the oil film transmits tractive forces, there will always be a certain degree of slip between them. The question that now arises is: Does the presence of sliding alter the situation? We know that film thickness, whether starved or flooded, is associated with the pressure generated in the inlet region. Furthermore, Reynolds equation implies that equivalent pressure distributions will be generated for both sliding and rolling pro-

vided the sum of the surface velocities are the same. Therefore, if sliding does not alter the pressure distribution, then the starvation behavior with respect to film thickness should be the same for sliding as well as rolling.

This is shown in Fig. 7 where measurements of film thickness under starved conditions were obtained for relative surface velocities ranging from pure rolling to 100 percent sliding. In Fig. 7 the dimensionless film thickness $h_f/(h_o)_f$ is plotted as a function of the inlet gap ratio h_f/h_o as well as the starvation parameter S/S_f defined as

$$\frac{S}{S_f} = \frac{S a^{4/3}}{3.52 [R(h_o)_f]^{2/3}}$$

The location of the inlet lubricant boundary can be defined in terms of h_o or S as shown in Fig. 8 where h_o is the gap thickness at the location of the inlet lubricant boundary and S is the inlet distance measured from the leading edge of the Hertz region to the inlet lubricant boundary. The derivation of this starvation parameter and the development of a starvation theory for film thickness under point contact conditions was obtained previously [1]. This starvation parameter is very similar to the one developed by Wolveridge, Baglin and Archard for line contact [3]. It has been shown that the starvation theories for line and point contact conditions are very similar [1]. The starvation parameter used here has the property that when its value is equal to one the inlet gap ratio $h_f/h_o = 9$. The corresponding film thickness under these conditions is 95 percent of its flooded value as shown by the theoretical curve in Fig. 7.

The experimental data for a wide range of sliding conditions agrees with theory as shown in Fig. 7. It can therefore be concluded that the starvation behavior with respect to film thickness is the same for both rolling and sliding conditions.

There are occasional references in the literature where the location of pressure commencement or the onset of starvation is associated with particular fluid velocity conditions within the inlet region such as the location where backflow begins [18-20], or the location of fluid rotation [21]. These conditions do not adequately define the onset of starvation and are not unique to both rolling and sliding [22]. For example, it can be shown that under pure rolling conditions backflow begins to occur upstream of the point where $h/h_0 = 3$. Under pure sliding conditions backflow begins to occur further downstream where $h/h_0 = 1.5$. The experimental and theoretical data of Fig. 7 shows clearly that the onset of starvation occurs much further upstream where $h/h_0 = 9$. This implies that a portion of the fluid in the inlet region flows backward with respect to the conjunction region and that this is a necessary condition to establish a fully flooded film.

STARVATION AND TRACTION

Traction is usually plotted in terms of the slide roll ratio which is defined as:

$$\text{slide roll ratio} = \frac{u_1 - u_2}{1/2 (u_1 + u_2)}$$

The denominator is the average velocity of the fluid passing through the Hertzian region and is by definition equal to the rolling velocity \bar{u} . The numerator is the sliding velocity between the ball and disk. At 100 percent sliding ($u_2 = 0$) the value of the slide roll ratio as defined above is two.

Traction measurements were performed under constant rolling velocity conditions; i.e., \bar{u} was kept constant for all values of the slide roll ratio. Fig. 9 shows the variation of traction force with the slide roll ratio for a maximum Hertzian pressure of $0.496 \times 10^9 \text{ N/m}^2$ (72,000 psi). The solid line which runs through the squares is the measured traction force under flooded conditions. The circles represent the traction force which was measured under various degrees of starvation. The significant feature of the results is that in all cases tested a starved film was observed to possess greater traction than a flooded film for the same slide roll ratio.

Fig. 10 shows the measured traction force performed at a maximum Hertzian pressure of $1.21 \times 10^9 \text{ N/m}^2$ (175,000 psi). At this pressure the traction force under flooded conditions rises more sharply and reaches a higher level. Here, again, we see that the traction forces measured under various degrees of starvation are in all cases higher than its corresponding flooded value for the same slide roll ratio. It is significant to note that very high traction forces can be achieved for very small values of sliding when the film is starved.

Fig. 11 shows the measured traction force performed at a maximum Hertzian pressure of $1.90 \times 10^9 \text{ N/m}^2$ (275,000 psi). The pattern of results is essentially the same as before.

It was noted here as well as the previous traction tests that relatively high traction forces were measured when the condition of 100 percent sliding was reached. This is caused by a greater degree of starvation which was always observed to accompany large amounts of sliding. In other words, sliding was found to be more prone to starvation than rolling.

The practical implication of this is that it can lead to an unstable condition if one surface is driving another as is the case here as well as many practical devices. This traction instability can be seen in Fig. 12 which shows the recorded traces of disk speed and traction force as a function of time. When the bearing becomes starved the traction force increases causing the disk to run faster. The faster disk rotation increases the rolling velocity \bar{u} and feeds more lubricant into the inlet region, both of which increase the film thickness which in turn decreases the traction. This causes the disk to slow down again. As this process continues the disk rotation "hunts" as shown in Fig. 12.

DISCUSSION OF STARVATION AND TRACTION RESULTS

The influence of starvation on film thickness has been successfully analyzed by normalizing film thickness and the location of the inlet boundary using their corresponding values under flooded conditions [1]. Hence, we obtained the dimensionless film thickness parameter $h_o/(h_o)_f$ and the dimensionless inlet boundary parameter S/S_f . These parameters generalize the starved EHD problem for other conditions of operation. The influence of starvation on traction is more difficult to analyze in this way. The reasons are the same as those which make it more difficult to predict traction than film thickness under flooded conditions. Except at very low sliding speeds the problem can no longer be considered isothermal and the rheological behavior of the fluid becomes complicated and ill-defined.

The influence of starvation on traction would be easy to predict if we could assume isothermal conditions and a Newtonian fluid. Traction would then be proportional to the shear rate in the Hertz region and

therefore inversely proportional to film thickness. The increase in traction over and above a flooded condition could then be directly related to the starvation parameter S/S_f . We would then find the traction force approaching infinity as the film thickness approaches zero which obviously does not represent reality.

Traction is influenced by starvation primarily by the shear conditions which it develops in the Hertz region. That is, a starved or thinner film increases the shear rate in the Hertz region for a given slide roll ratio. These same shear conditions govern heat generation and non-Newtonian behavior. It is for this reason that the traction results will be considered in terms of the apparent shear rate defined as $(u_1 - u_2)/h_o$.

Fig. 13 shows the measured traction force as a function of the shear rate for all the test conditions. The solid curves represent the traction under flooded conditions. The form of the flooded curves are the same as those in Figs. 9,10 and 11. The dashed curves represent the traction measured under starved conditions. The distinguishing feature between the starved and flooded results is that under flooded conditions the shear rate reaches a limiting value at 100 percent sliding whereas a starved film can produce very much higher shear rates than a flooded one. In fact, there is no theoretical limit. The maximum traction force under starved conditions will very much depend on the rheological properties of the fluid and the thermal conditions that prevail in the conjunction region.

One of the major reasons for looking at the results in terms of shear rate is that we are essentially normalizing the flooded and starved results in terms of heat generation. For example, it can be shown that

the heat generation within the film is proportional to the square of the shear rate $(u_1 - u_2)/h_c$. What this means is that for a given shear rate the heat generation should be about the same for a flooded film as it is for a starved film. The temperature of the film, however, depends on heat conduction to the surfaces. Since a starved, or thinner, film will have better heat conduction than a flooded or thicker film we should expect the measured traction under starved conditions to be higher than a flooded condition for the same shear rate. Fig. 13 shows this to be the case in the region where the shear rate is moderately high.

However, when the shear rates in the Hertz region are low and the film is severely starved much lower traction forces were measured than expected. This is shown in Figs. 14, 15 and 16, where the region of low shear rate has been expanded. The solid curves again represent the traction under flooded conditions. The broken curves show the traction under various degrees of starvation. The unexpected feature of the results is that as the shear rate becomes smaller and the oil film in the Hertz region becomes more starved, the measured traction force becomes very much lower than the flooded value. This is particularly noticeable under the highest Hertzian pressure shown in Fig. 16. These results are contrary to what could be expected when the influence of starvation on traction is considered in terms of film thickness changes in the Hertz region along with the expected trends in heat generation and dissipation. There appears to be an additional factor (or factors) which influences traction under severely starved conditions.

In addition to film thickness, starvation influences other EHD operating conditions. For example, starvation causes the pressure distribution and elastic deformation to become more Hertzian [1]. Intuitively, this would not explain a reduction in traction force for the same shear rate. Starvation also causes a reduction in rolling friction since less pressure is generated in the inlet region [4]. The traction measurements, however, did not include rolling friction.

A tentative explanation may be put forward if one considers the effect of starvation on the shear conditions in the inlet region and the recent evidence of Adams and Hirst [23] who have associated the high shear stresses in the inlet region with non-Newtonian behavior in this region. Under flooded conditions the pressure rises gradually in the inlet region and blends in smoothly with the Hertzian pressure. However, when the inlet region becomes starved the pressure starts much later and rises more rapidly. This has been shown by the full computer solution of Castle and Dowson [4] for the starved film thickness problem in line contact. In the limit, the pressure gradient approaches the very steep gradient of the Hertzian pressure distribution. Therefore, under severely starved conditions very high shear stresses must be associated with these severe pressure gradients. It is tentatively proposed here that these severe pressure gradients which occur in the inlet region when it is severely starved may influence the lubricant's traction performance in the Hertz region.

It can be argued that if the traction under starved conditions is influenced by high shear stresses in the inlet region, then film thickness must also be influenced by the same behavior. Although the film thickness

data of Fig. 7 appear to be somewhat lower than theory under severely starved conditions, it must be noted that the measurement of the location of the inlet boundary (S) becomes very difficult under severely starved conditions as shown in Fig. 6(c). The experimental error in the data of Fig. 7 is too great to make any comment on the effect of shear stress in the inlet region on film thickness under severely starved conditions.

EFFECT OF PRESSURE ON FILM THICKNESS

The three test pressures used here were obtained by using different material combinations which resulted in similar deformations in each case. Table 3 shows that the rolling velocities necessary to obtain a film thickness corresponding to the third red fringe are similar for each test pressure. The sensitive effect of Hertz pressure on film thickness was not observed here as it was elsewhere [11] for line contact under much higher rolling velocities. This is shown in Fig. 17 where the central film thickness h_o and the film thickness at the rear (h_r) and side (h_g) constrictions are plotted as a function of the maximum Hertzian pressure. These measurements were performed with the sapphire/steel materials combination under pure rolling conditions with the same lubricant used for the traction measurements. The absolute value of the central film thickness as well as its variation with pressure agrees with film thickness theory [1] which is plotted in Fig. 17. The film thickness at the side constrictions (h_g) which occur for different reasons than the rear constriction is more sensitive to pressure than h_o or h_r . This has been observed elsewhere [24].

CONCLUSIONS

Traction and film thickness measurements under starved EHD rolling and sliding conditions have been made for a point contact geometry. The variation of film thickness with the location of the inlet lubricant boundary under combination rolling and sliding behaves identically with that found previously under pure rolling conditions. This is expected if one considers the commencement of pressure generation in Reynolds equation in terms of the inlet gap geometry defined by h/h_0 . This ratio defines the location of various fluid velocity conditions within the inlet region. These velocity conditions do not adequately define the onset of starvation. It is furthermore concluded that backflow occurs over a portion of the inlet pressure buildup and that this is a necessary condition for the establishment of a fully flooded film.

In all cases tested, a starved film was observed to possess greater traction than a flooded film for the same slide roll ratio. For a given slide roll ratio a starved film simply increases the shear rate in the Hertz region. The maximum shear rate depends on the degree of starvation and has no theoretical limit.

The relative increase in traction due to starvation for a given slide roll ratio depends primarily on the thermal and fluid rheological conditions within the Hertz region. It is for this reason that the prediction of traction under starved conditions cannot easily be achieved by normalizing the traction under starved conditions with its corresponding flooded condition at the same slide roll ratio. Thus, traction measurements were considered in terms of the shear rate $(u_1 - u_2)/h_0$ within the Hertz region. In this way the flooded and starved traction measurements

could be compared under conditions of similar heat generation. Except for low rates of shear, the measured tractions under starved conditions were found to be greater than the traction under flooded conditions for the same shear rate. This can be explained in terms of improved heat conduction when the film is thinner or starved.

When the shear rates in the Hertz region were low and the film severely starved, the measured tractions were found to be much lower than expected. It is tentatively suggested that this may be explained in terms of the high shear stresses developed by the large pressure gradient which occurs within the inlet region when it is severely starved. Thus, the shear history of the fluid in the inlet region may affect the traction developed in the Hertz region.

REFERENCES

1. Wedeven, L. D., Evans, D., and Cameron, A., "Optical Analysis of Ball Bearing Starvation," Journal of Lubrication Technology, Trans. ASME, Series F, Vol. 93, No. 3, July 1971, pp. 349-363.
2. Orcutt, F. A., and Cheng, H. S., "Lubrication of Rolling-Contact Instrument Bearings," Proc. Gyro Spin-Axis Hydrodynamic Bearing Symposium, Vol. II, Chap. 5, M.I.T., Mass., 1966, pp. 1-25.
3. Wolveridge, P. E., Baglin, K. P., and Archard, J. F., "The Starved Lubrication of Cylinders in Line Contact," Proc. Instr. Mech. Engrs., Vol. 185, 1970-1971, pp. 1159-1169.
4. Castle, P., and Dowson, D., "A Theoretical Analysis of the Starved Elastohydrodynamic Lubrication Problem for Cylinders in Line Contact," Instr. Mech. Engrs. Papers C35/72, Apr. 1972.
5. Smith, R. L., and McGrew, J. M., "Failure Modes and Accelerated Life Test Methods for Deepgroove Antenna Bearings," Lubrication Engineering, ASLE, Vol. 30, No. 1, Jan. 1974, pp. 17-26.
6. Horsch, J. D., "Correlation of Gyro Spin-Axis Ball Bearing Performance with the Dynamic Lubricating Film," Trans. ASLE, Vol. 6, 1963, pp. 112-124.
7. Münnich, H., "Einfluss der Schmierung auf Lebensdauer, Reibung und Verschleiss von Wälzlagern," Schmieretechnik und Tribologie, Vol. 16, No. 2, 1968, pp. 87-97.
8. Popinceanu, N. G., et al., "A Study of Rolling Bearing Fatigue Life with Mineral Oil Lubrication," Wear, Vol. 22, 1972, pp. 21-37.
9. Foord, C. A., et al., "Optical Elastohydrodynamics," Proc. Inst. Mech. Engrs., Vol. 184, Pt. 1, No. 28, 1969-70, pp. 487-505.

10. Carlson, S., et al., "Investigation of Lubricant Rheology as Applied to Elastohydrodynamic Lubrication," Georgia Institute of Technology, 1973 (also NASA CR-134539).
11. Parker, R. J., and Kannel, J. W., "Elastohydrodynamic Film Thickness Between Rolling Disks With a Synthetic Paraffinic Oil to 589 K (600° F)," NASA TN D-6411, July 1971.
12. Trachman, E. G., and Cheng, H. S., "Rheological Effects on Friction in Elastohydrodynamic Lubrication," NASA CR-2206, Mar. 1973.
13. Rhoads, W. L., and Peacock, L. A., "Advanced Turbine Engine Mainshaft Lubrication System Investigation, Phase 2. Part 1: Background, Test Elements and Results, and Conclusions for System Performance," AL69T016, SKF Industries, Inc., 1971 (also NASA CR-72854).
14. Loomis, W. R., Townsend, D. P., and Johnson, R. L., "Lubricants for Inerted Lubrication Systems in Engines for Advanced Aircraft," SAE Paper No. 680317, May 1968.
15. Rhoads, W. L., and Sibley, L. B., "Supersonic Transport Lubrication System Investigation, Phase 1," AL67T060, SKF Industries, Inc., 1967 (also NASA CR-54662).
16. Chiu, Y. P., Hahn, D., and Rosenberg, N., "Exploratory Analysis of Elastohydrodynamic Properties of Lubricants," AL72P001, SKF Industries, Inc., 1971.
17. Wymer, D., "Discussion," Proc. Instr. Mech. Engrs., FHD Symposium, Leeds, Apr. 1972, p. 197.
18. Lauder, W., "Hydrodynamic Lubrication of Proximate Cylindrical Surfaces of Large Relative Curvature," Proc. Inst. of Mech. Engrs., Vol. 180, Pt. 3B, 1965-66, pp. 101-106.

19. Whitaker, A. V., "Communication," Proc. Inst. Mech. Engrs., Vol. 180, Pt. 3B, 1965-66, p. 246.
20. Capone, E., DeRosa, E., and Migliaccio, M., "A Study of the Lubrication of Discs," Wear, Vol. 22, 1972, pp. 91-103.
21. Tipei, N., "Boundary Conditions of a Viscous Flow Between Surfaces With Rolling and Sliding Motion," Journal of Lubrication Technology, Trans. ASME, Series F, Vol. 90, No. 1, Jan. 1968, pp. 254-261.
22. Wedeven, L. D., Effect of Starvation on Film Thickness and Traction Under Elastohydrodynamic Rolling and Sliding Conditions. NASA TN to be published.
23. Adams, D. R., and Hirst, W., "Frictional Traction in Elastohydrodynamic Lubrication," Proc. Roy. Soc. (London), Series A, Vol. 332, 1973, pp. 505-525.
24. Foord, C. A., Hammann, W. C., and Cameron, A., "Evaluation of Lubricants Using Optical Elastohydrodynamics," ASLE Trans., Vol. 11, No. 1, Jan. 1968, pp. 31-43.

E-8036

TABLE 1 - MECHANICAL PROPERTIES OF TEST MATERIALS

| Material | Compressive strength | | Modulus of elasticity | | Poisson's ratio | Specific heat | Thermal conductivity, cal/(sec)(cm ²)(°C)/cm at 20° C |
|------------------|----------------------|---------------------|-----------------------|----------------------|-----------------|---------------|---|
| | N/m ² | psi | N/m ² | psi | | | |
| Quartz | 1.14x10 ⁹ | 166x10 ³ | 70.3x10 ⁹ | 10.2x10 ⁶ | 0.17 | 0.20 | 0.0033 |
| Sapphire | 2.07x10 ⁹ | 300x10 ³ | 465x10 ⁹ | 67.5x10 ⁶ | 0.47 | 0.18 | 0.092 |
| Steel | 1.38x10 ⁹ | 200x10 ³ | 207x10 ⁹ | 30x10 ⁶ | 0.30 | 0.12 | 0.12 |
| Tungsten carbide | 5.16x10 ⁹ | 752x10 ³ | 641x10 ⁹ | 93x10 ⁶ | 0.25 | 0.03 | 0.041 |

TABLE 2. - PROPERTIES OF SYNTHETIC PARAFFINIC OIL

| | |
|---|---|
| Viscosity | |
| 37 000 cS | at 17.8° C (0° F) |
| 447 cS | at 37.8° C (100° F) |
| 40.4 cS | at 98.9° C (210° F) |
| 13 cS | at 149° C (300° F) |
| 6 cS | at 204° C (400° F) |
| Density | |
| 0.7428 g/ml | at 204° C (400° F) |
| 0.7777 g/ml | at 149° C (300° F) |
| 0.8082 g/ml | at 93.3° C (200° F) |
| 0.8389 g/ml | at 37.8° C (100° F) |
| Pressure-viscosity coefficient, ^a α | |
| 0.931 N/m ² | (1.35x10 ⁻⁴ (psi) ⁻¹) at 38° C (100° F) |
| 0.738 N/m ² | (1.07x10 ⁻⁴ (psi) ⁻¹) at 99° C (210° F) |
| 0.593 N/m ² | (0.86x10 ⁻⁴ (psi) ⁻¹) at 149° C (300° F) |
| Refractive index | |
| 1.4689 | at 26° C (78.8° F) |
| Flash point | |
| 271° C | (520° F) |
| Fire point | |
| 313° C | (595° F) |
| Pour point | |
| -51° C | (-60° F) |
| Specific heat | |
| 0.635 | at 149° C (300° F) |
| 0.692 | at 204° C (400° F) |
| Surface tension | |
| 30.3 dynes/cm | |

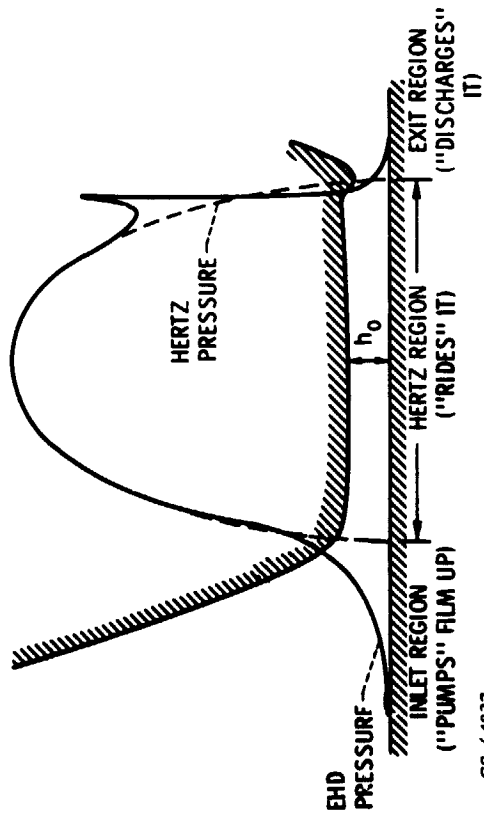
^aFrom ref.10 and defined as $(\alpha)^{-1} = \int_0^{\infty} \mu_c dp / \mu(p)$.

E-8036

TABLE 3. - TEST CONDITIONS

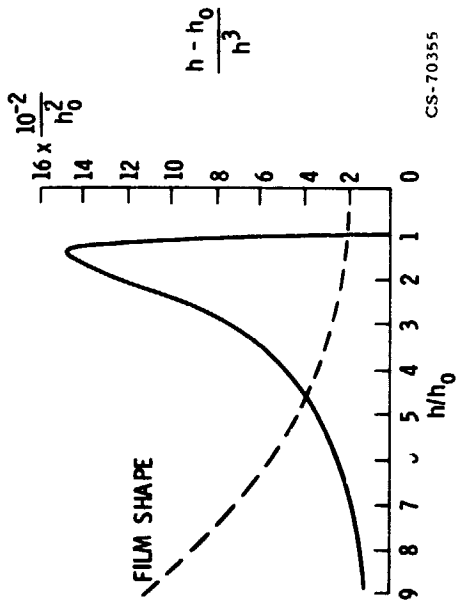
| | Test no. 1 | Test no. 2 | Test no. 3 |
|--|---|---|---|
| Maximum Hertz pressure, (p_{max}) | 0.496×10^9 N/m ² 72 000 psi | 1.21×10^9 N/m ² 175 000 psi | 1.90×10^9 N/m ² 275 000 psi |
| Load | 22.3 N 5 lbf | 37.8 N 8.5 lbf | 36.7 N 8.25 lbf |
| Hertz radius (a) | 0.149×10^{-3} m 5.87×10^{-3} in. | 0.121×10^{-3} m 4.77×10^{-3} in. | 0.096×10^{-3} m 3.79×10^{-3} in. |
| Material combination | Quartz/steel | Sapphire/steel | Sapphire/tungsten carbide |
| Rolling velocity $u = \frac{1}{2}(u_1 + u_2)$ | 0.1366 m/s 5.38 in./s | 0.1540 m/s 6.06 in./s | 0.1554 m/s 6.12 in./s |
| Test temperature | 23.5° C 74.3° F | 24° C 75.2° F | 24° C 75.2° F |
| $S_f = \frac{3.52(Rh_o)^{2/3}}{a^{1/3}}$ | 0.222×10^{-3} m 8.74×10^{-3} in. | 0.23×10^{-3} m 9.06×10^{-3} in. | 0.241×10^{-3} m 9.49×10^{-3} in. |
| Flood film thickness (h_o) _f | 0.592 μm 23.3 μin. | 0.562 μm 22.1 μin. | 0.538 μm 21.2 μin. |

E-8036



CS-64827

Figure 1. - The three general regions of the EHD conjunction.



CS-70355

Figure 2. - The geometry term $(h - h_0)/h^3$ as a function of the dimensionless gap ratio h/h_0 .



CS-70225

Figure 3. - Test ball, transparent disk and lubricant reservoir.

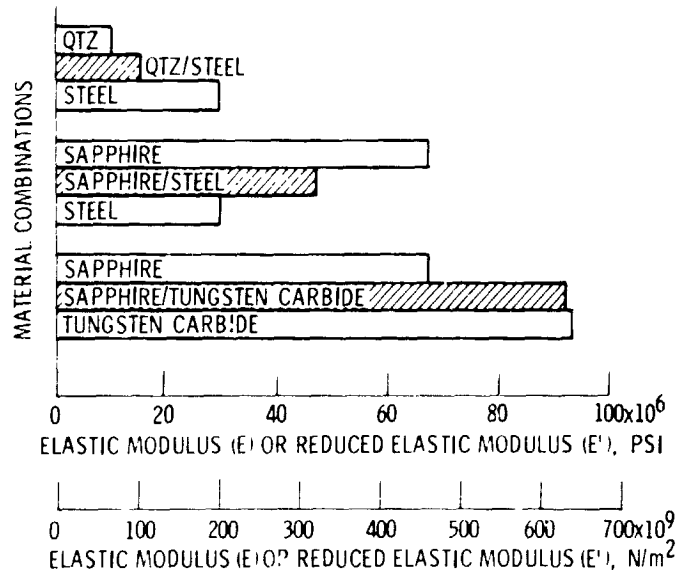
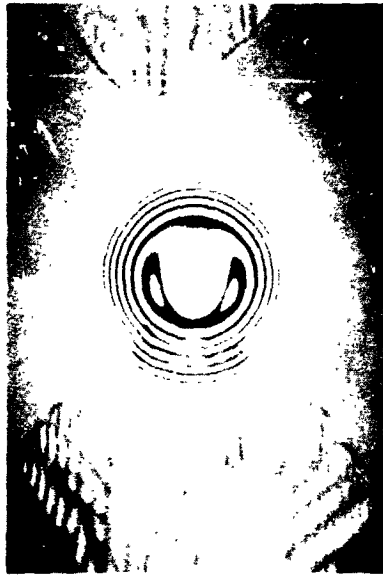


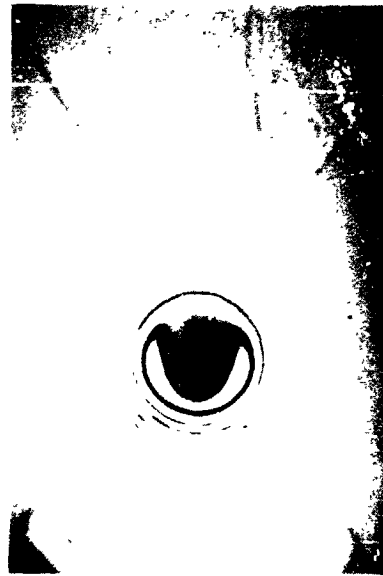
Figure 4. - Elastic modulus and reduced elastic modulus for test materials.



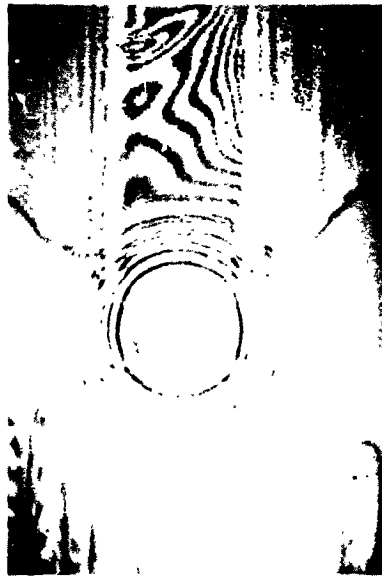
Figure 5. - The apparatus.



(a) $S = .259 \times 10^{-3}$ m, $h_0 = .50$ μ m,
 $\bar{u} = .155$ m/s, $u_1 - u_2 = .156 \times 10^{-2}$ m/s,
 traction force = 1.0 N.



(b) $S = .091 \times 10^{-3}$ m, $h_0 = .370$ μ m,
 $\bar{u} = .153$ m/s, $u_1 - u_2 = .722 \times 10^{-2}$ m/s,
 traction force = 1.84 N.



(c) $S = .023 \times 10^{-3}$ m, $h_0 = .08$ μ m,
 $\bar{u} = .1556$ m/s, $u_1 - u_2 = .3112$ m/s (pure
 sliding), traction force = 3.22 N.

Figure 6. - Typical photomicrographs showing effect of starvation on film thickness;
 materials, sapphire/tungsten carbide; load, 36.7 N; $P_{max} = 1.90 \times 10^7$ N/m² (275,000
 psi); $(h_0)_f = .538$ μ m.

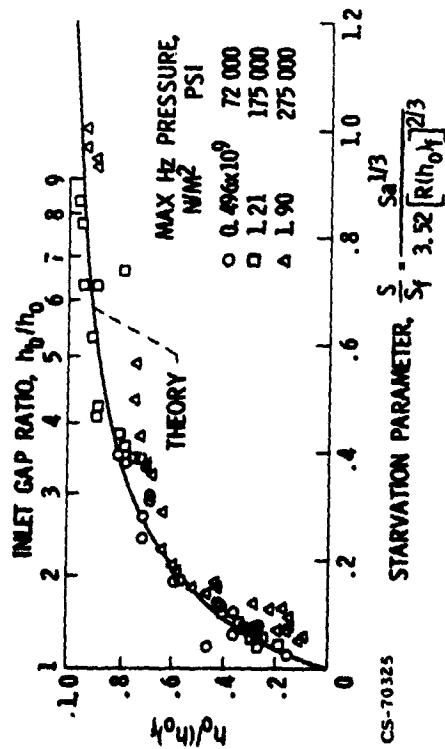


Figure 7. - Variation of film thickness with starvation for rolling and sliding conditions.

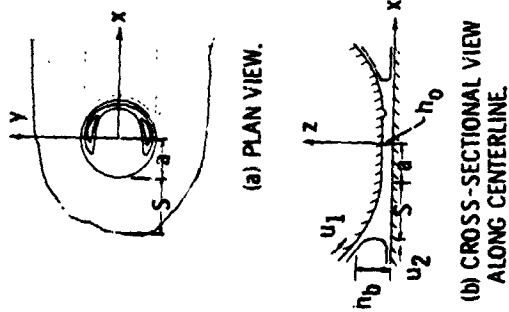


Figure 8. - Contact geometry showing required measurements for starvation.

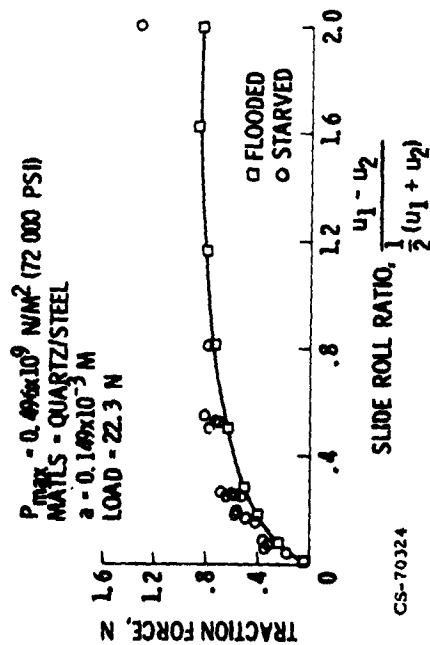


Figure 9. - Variation of traction with slide roll ratio under starved and flooded conditions, $P_{max} = 72 \text{ 000 psi}$.

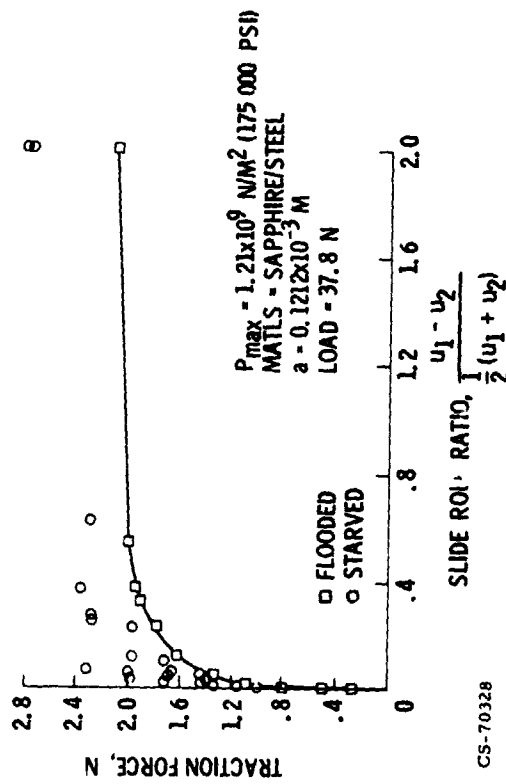


Figure 10. - Variation of traction with slide roll ratio under starved and flooded conditions, $P_{max} = 175 \text{ 000 psi}$.

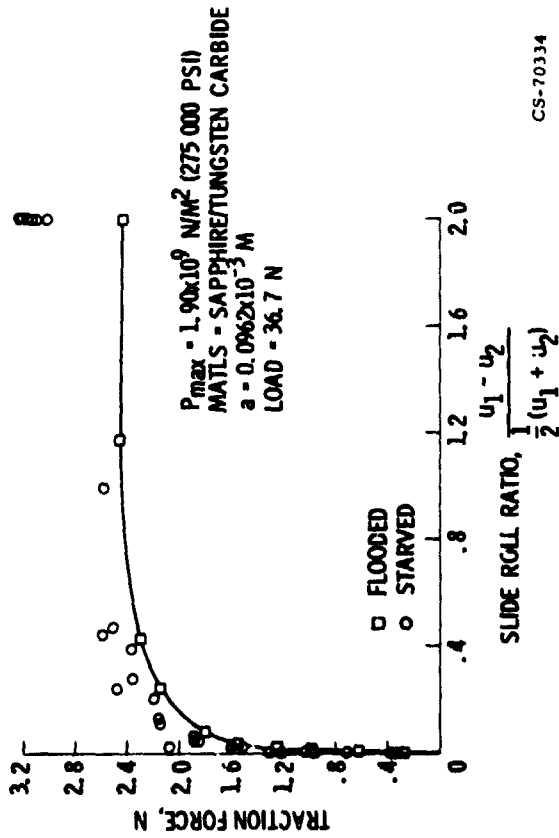


Figure 11. - Variation of traction with slide roll ratio under starved and flooded conditions. $P_{max} = 275 \text{ 000 psi}$.

CS-70334

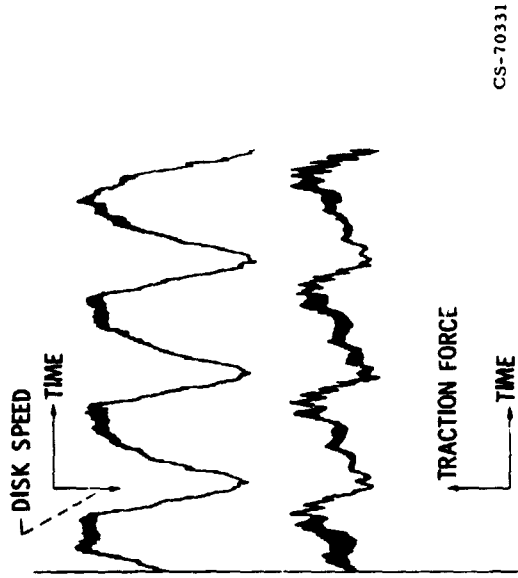


Figure 12. - Traction and disk speed under unstable starvation conditions.

CS-70331

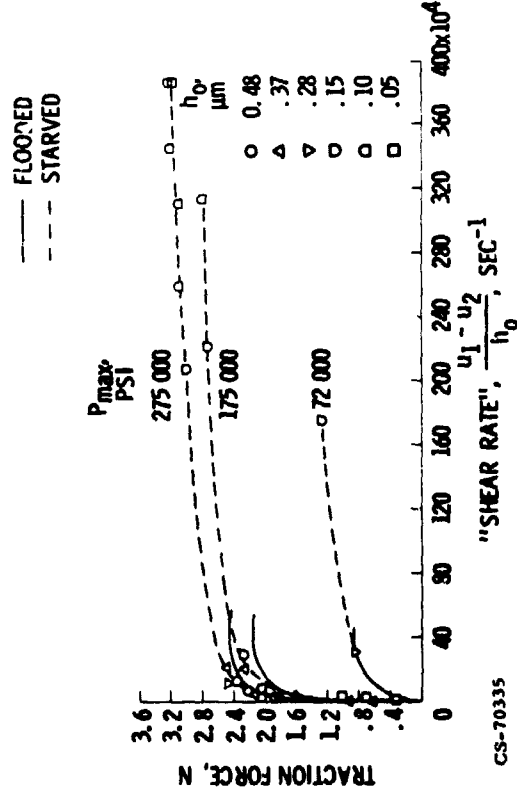


Figure 13. - Variation of traction with shear rate for starved and flooded conditions.

CS-70335

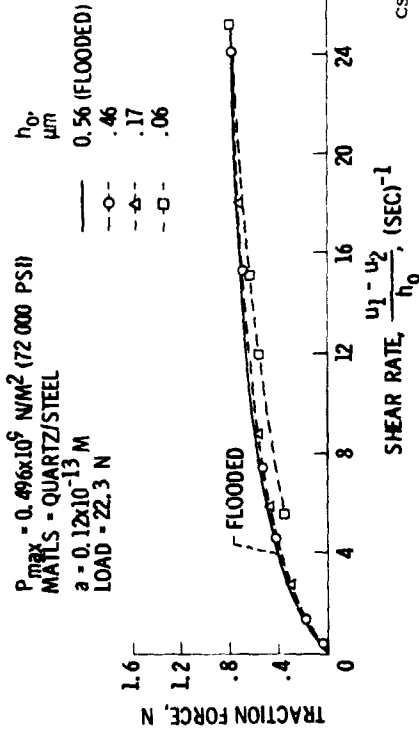


Figure 14. - Variation of traction with shear rate under starved and flooded conditions. $P_{max} = 72 \text{ 000 psi}$.

CS-70333

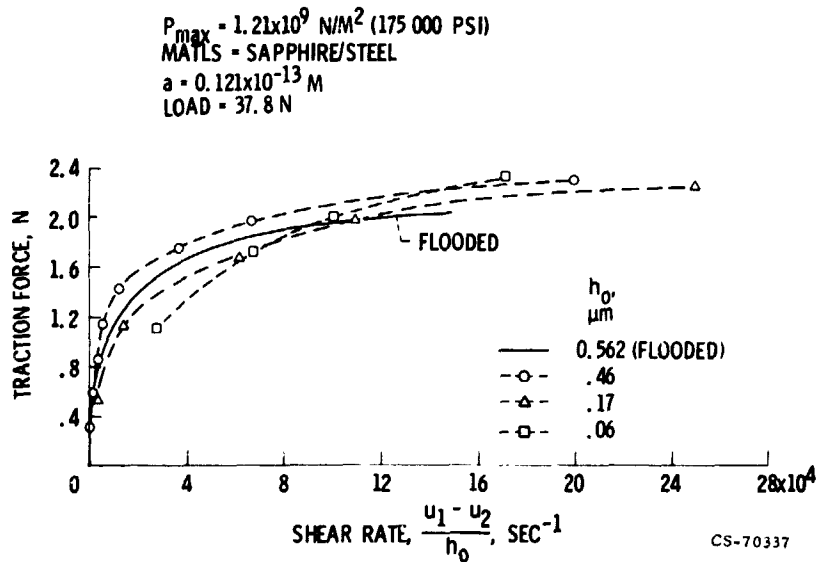


Figure 15. - Variation of traction with shear rate under starved and flooded conditions, $P_{max} = 175\ 000$ psi.

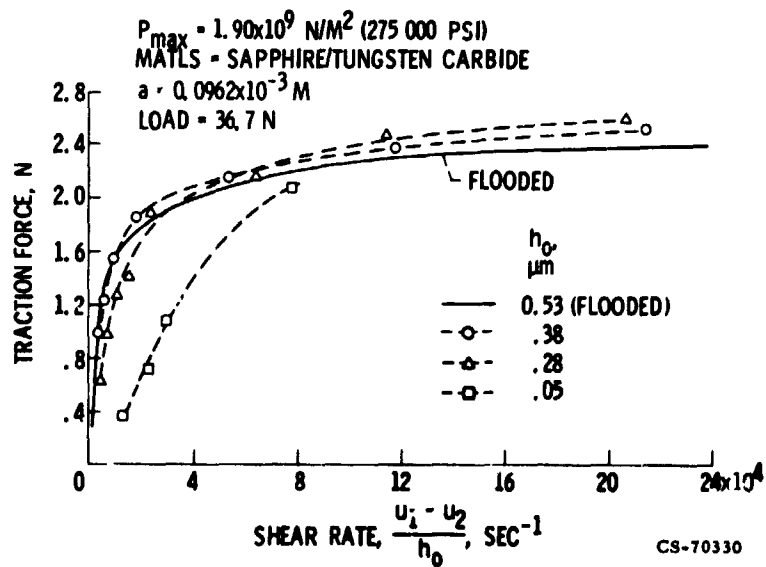
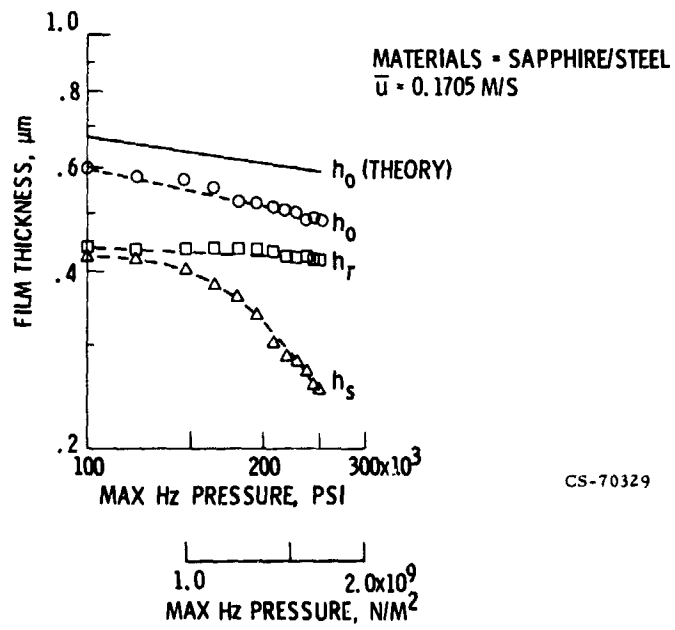


Figure 16. - Variation of traction with shear rate under starved and flooded conditions, $P_{max} = 275\ 000$ psi.

E-8036



CS-70329

Figure 17. - Effect of maximum Hertz pressure on film thickness.